$BaSr(Al_{0.5}Nb_{0.5})O_3$ Perovskite Nanoparticles: Structural and Optical Evaluation for Efficient Light Absorber Layers in Solar Cells

Deepak M. Sonawane[1], Anil N. Kalyankar[2], Pratik P. Raut[3], Karankumar R. Sature[1], Sunil J Indurkar[1], Yogesh K lahamate[1], Abhijit C Bhagat[1], Nikhil M. Ghumbare[4], Shivnarayan B. Bajaj[1]

[1]Department of Physics, J. E. S., R.G. Bagdia Arts, S.B. Lakhotia Commerce & R, Benzoji Science College, Jalna, (MS) India.
[2]Department of Physics, Bahirji Smarak Mahavidyalaya, Basmath, Dist. Hingoli, (MS) India.
[3]Department of Physics, DSM ACS College Parbhani, 431401, (MS) India.
[4]Department of Physics, Shri Shivaji college, Parbhani 431401, (MS) India.

Abstract: In this work, $BaSr(Al_{0.5}Nb_{0.5})O_3$ (BSAN) perovskite nanoparticles were synthesized using the solid-state reaction method and evaluated for potential application in solar cells. XRD confirmed the formation of a single-phase cubic perovskite structure with crystallite sizes between 33 nm and 55 nm. FTIR analysis indicated characteristic metal–oxygen vibrations, confirming phase formation. SEM analysis revealed uniform, granular nanoparticles with sizes predominantly in the 30–70 nm range. BET surface area analysis exhibited a high specific surface area of 58.4 m^2/g and mesoporosity. EDS confirmed elemental homogeneity without impurities. UV-Vis spectroscopy showed strong visible light absorption with an optical bandgap of 1.56 eV, suitable for efficient solar energy harvesting. The combined results highlight BSAN's suitability as an absorber layer or electron transport layer in photovoltaic devices.

Keywords: $BaSr(Al_{0.5}Nb_{0.5})O_3$, Perovskites, Solid-State Reaction, Optical Bandgap, Solar Cells

1. Introduction

Perovskite materials with the general formula ABO_3 have attracted considerable attention in recent years due to their unique structural versatility and multifunctional properties, making them highly relevant in renewable energy technologies. The ABO_3 perovskite structure allows for a wide variety of elemental substitutions at both A and B sites, offering tunable electrical, optical, and magnetic properties that are suitable for various applications such as solar cells, fuel cells, supercapacitors, and catalysis[1]. These materials exhibit excellent features such as high dielectric constants, strong light absorption, and favourable charge transport properties, which are essential for efficient energy conversion and storage.
Several researchers have highlighted the significance of perovskite materials in the advancement of energy technologies. For instance, Zhu et al. (2016) demonstrated that tuning cation deficiency in perovskite oxides significantly enhances their electrocatalytic performance, particularly in oxygen reduction and evolution reactions, crucial for energy storage and fuel cell applications [2]. Similarly, Caliò et al. (2016) underscored the importance of hole-transport materials (HTMs) in perovskite solar cells to facilitate efficient charge extraction and minimize recombination losses, which are key factors in improving solar cell efficiency [3]. The versatility of perovskite oxides has also been emphasized by Sunarso et al. (2017), who reviewed their applications in high-temperature oxygen separation membranes, solid oxide fuel cells, and catalytic membrane reactors. These studies collectively highlight the potential of perovskites in various domains of renewable energy [4].
Recent advancements have also focused on hybrid perovskite materials in photovoltaic applications. Anzolin et al. (2018) discussed the promising future of hybrid perovskite solar cells, emphasizing their ability to redefine the value chain of photovoltaics by offering low-cost, high-efficiency solutions [5]. Furthermore, Kamaraki et al. (2021) explored the integration of perovskite materials with conventional silicon technologies to develop tandem solar cells, combining the advantages of both materials to

achieve higher energy conversion efficiencies and increased solar deployment rates [6]. The translation of such cutting-edge materials research into scalable industrial processes has been addressed by Wei et al. (2024), who stressed the need to bridge scientific innovation with practical manufacturing techniques to accelerate the commercialization of perovskite photovoltaics [7].

In light of this, the present study focuses on the synthesis and characterization of $BaSr(AlNb)O_3$ perovskite nanoparticles, a novel composition selected for its potential advantages in photovoltaic applications [8]. The choice of $BaSr(AlNb)O_3$ is motivated by the favorable structural stability imparted by the Ba and Sr ions at the A-site, coupled with the ability of Al and Nb at the B-site to modulate the material's electronic and optical properties [9]. The substitution of these cations is anticipated to influence the band structure, dielectric properties, and charge carrier mobility, all of which are critical for enhancing solar cell performance.

The use of perovskite nanoparticles, in particular, offers additional benefits for solar energy applications. Reducing the particle size to the nanoscale increases the surface area-to-volume ratio, shortens charge diffusion lengths, and improves interface quality in device architectures, leading to better light absorption and charge collection efficiencies [10]. Moreover, nanoparticles can be easily incorporated into flexible and lightweight photovoltaic devices, broadening the scope for next-generation solar technologies.

For the synthesis of $BaSr(AlNb)O_3$ nanoparticles, the solid-state reaction route was chosen due to its simplicity, cost-effectiveness, scalability, and ability to produce phase-pure crystalline materials with controlled stoichiometry. Unlike wet-chemical methods, the solid-state approach involves direct reaction of high-purity precursors at elevated temperatures without the need for solvents or complex processing steps, making it well-suited for large-scale production and industrial applications [11].

The primary objectives of this research are to successfully synthesize $BaSr(AlNb)O_3$ perovskite nanoparticles using the solid-state reaction method and to systematically characterize their structural, morphological, optical, and surface properties. Various analytical techniques, including X-ray diffraction (XRD), Fourier-transform infrared spectroscopy (FTIR), scanning electron microscopy (SEM), energy-dispersive X-ray spectroscopy (EDS), UV-Vis spectroscopy, and Brunauer–Emmett–Teller (BET) surface area analysis, have been employed to comprehensively investigate the properties of the synthesized nanoparticles [12]. Furthermore, the suitability of $BaSr(AlNb)O_3$ nanoparticles for solar cell applications is evaluated based on the obtained characterization results, with a focus on their potential to contribute to the development of efficient and sustainable photovoltaic technologies [13], [14].

2. Experimental

2.1 Materials and Chemicals

$BaSr(Al_{0.5}Nb_{0.5})O_3$ perovskite nanoparticles were synthesized via the conventional solid-state reaction method using high-purity starting materials. The precursor materials used in this synthesis included barium oxide (BaO, 99% purity), strontium oxide (SrO, 99% purity), aluminum oxide (Al_2O_3, 99.9% purity), and niobium pentoxide (Nb_2O_5, 99.9% purity) [15]. All chemicals were procured from LOBA Chemie Pvt. Ltd., India, and used as received without any further purification to maintain the desired stoichiometry and ensure high product purity.

2.2 Synthesis Procedure

The synthesis of $BaSr(Al_{0.5}Nb_{0.5})O_3$ was carried out via the solid-state reaction route. Stoichiometric quantities of BaO, SrO, Al_2O_3, and Nb_2O_5 were accurately weighed according to the molar ratio required for the $BaSr(Al_{0.5}Nb_{0.5})O_3$ composition. The weighed precursor powders were mixed thoroughly using an agate mortar and pestle to achieve uniform distribution of the constituent elements [16]. During the mixing process, acetone was added as a wetting agent to promote homogeneity and facilitate effective interaction between the reactants. The grinding process was continued for 3 hours to obtain a finely mixed and homogeneous precursor powder.

The homogenized powder mixture was subjected to a pre-calcination process at a temperature of 800°C for 6 hours in an air atmosphere [17]. This step facilitated the decomposition of any carbonate species, removal of volatile impurities, and initiation of solid-state diffusion reactions. After pre-calcination, the powder was allowed to cool naturally to room temperature inside the furnace.

Following the pre-calcination step, the material was reground to break down any agglomerates formed during heating and to further enhance the uniformity of the mixture. The reground powder was then subjected to the final sintering process at 1200°C for 16 hours in an air atmosphere to ensure the complete formation of the perovskite $BaSr(Al_{0.5}Nb_{0.5})O_3$ phase. The sintered material was cooled gradually to room temperature inside the furnace to prevent thermal stresses and structural defects [18]. The final product was collected in the form of a fine, homogeneous powder and stored in airtight containers to prevent moisture absorption and contamination. The synthesized $BaSr(Al_{0.5}Nb_{0.5})O_3$ powder was used for subsequent structural, morphological, optical, and surface area characterizations [19].

3. Results and Discussion

3.1 X-ray Diffraction (XRD) Analysis

The crystalline structure and phase purity of the synthesized $BaSr(Al_{0.5}Nb_{0.5})O_3$ (BSAN) nanoparticles were confirmed through X-ray diffraction (XRD) analysis. The recorded XRD pattern of BSAN nanoparticles is shown in Figure 1, where prominent diffraction peaks are observed at 2θ values of 28.88°, 30.86°, 34.33°, 42.80°, 49.91°, 54.90°, 64.34°, 68.88°, and 72.06°. These peaks correspond to the (110), (101), (111), (200), (201), (211), (202), (300), and (301) crystallographic planes of the cubic perovskite structure, respectively. The sharpness and intensity of the peaks indicate the formation of a highly crystalline and phase-pure perovskite material without any detectable secondary phases [20].

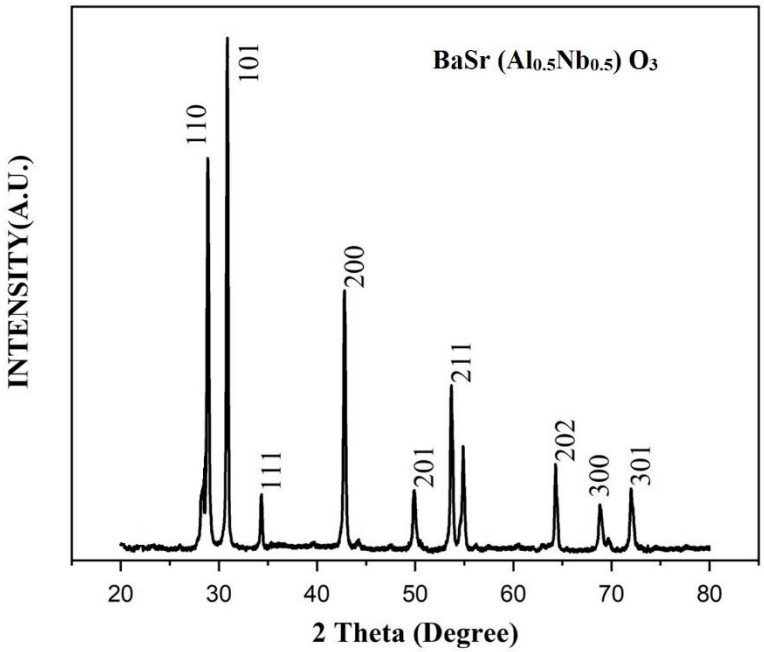

Figure 1: XRD pattern of BSAN perovskite nanoparticles

The crystallite size (D) of the BSAN nanoparticles was estimated using the Debye-Scherrer formula:

$$D = \frac{K\lambda}{\beta\cos\theta}$$

where K is the shape factor (0.9), λ is the wavelength of Cu-Kα radiation (1.5406 Å), β is the full width at half maximum (FWHM) of the peaks in radians, and θ is the Bragg angle. The calculated crystallite sizes from various peaks ranged between 26.34 nm and 41.3 nm, confirming the nanocrystalline nature of the synthesized BSAN.

The lattice constant (a) for the cubic structure was calculated using:

$$a = d \times \sqrt{h^2 + k^2 + l^2}$$

where d is the interplanar spacing derived from Bragg's equation. The calculated lattice constants varied consistently between 4.08 Å to 4.52 Å, which are in good agreement with the standard cubic perovskite lattice parameters. These values support the successful formation of a cubic BSAN phase [21].

$$\beta\cos\theta = \frac{K\lambda}{D} + 4\epsilon\sin\theta$$

where ε is the microstrain in the lattice. The Williamson-Hall plot for BSAN nanoparticles, shown in Figure 2, illustrates the linear relationship between βcosθ and 4sinθ. From the slope and intercept of the fitted line, the microstrain and crystallite size were obtained [22]. The W-H method yielded an average crystallite size of 55.67 nm, which is slightly larger than that calculated via Scherrer's equation due to the incorporation of strain contributions. The microstrain was calculated to be 0.0026, indicating minimal lattice distortion.

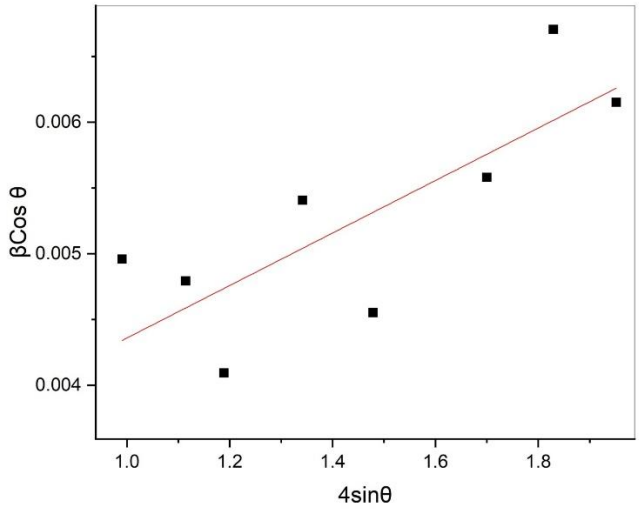

Figure 2: Williamson-Hall plot of BSAN nanoparticles

Additionally, the dislocation density (δ), representing the number of defects and dislocations within the crystal lattice, was calculated using the relation:

$$\delta = \frac{1}{D^2}$$

The dislocation density values ranged between 5.86×10^{14} lines/m² and 14.41×10^{14} lines/m², as listed in Table 1. Lower dislocation density values correlate with better crystallinity and reduced structural imperfections, which are crucial for optoelectronic performance.

A detailed summary of the XRD analysis parameters, including 2θ values, FWHM, d-spacing, Miller indices, crystallite size, lattice constants, strain, and dislocation density, is provided in Table 1. The consistent lattice constant values, low strain, and low defect density confirm the high crystalline quality of the BSAN nanoparticles [23].

Table 1: XRD Parameters of BSAN Nanoparticles

2θ (°)	FWHM (°)	d-spacing (Å)	(hkl)	Crystallite Size D (nm)	Lattice Constant a (Å)	Strain (ε)	Dislocation Density δ (10^{14} lines/m²)
28.88	0.2469	3.0875	110	33.20	4.3664	0.00418	9.08
30.86	0.1994	2.8944	101	41.30	4.0933	0.00315	5.86
34.33	0.2045	2.6092	111	40.64	4.5192	0.00289	6.05
42.80	0.2590	2.1102	200	32.92	4.2204	0.00288	9.23
49.91	0.3242	1.8250	201	27.01	4.0808	0.00304	13.71
54.90	0.3183	1.6705	211	28.11	4.0919	0.00267	12.66
64.34	0.2899	1.4462	202	32.36	4.0905	0.00201	9.55
68.88	0.3655	1.3615	300	26.34	4.0845	0.00233	14.41
72.06	0.3652	1.3092	301	26.89	4.13996	0.00219	13.82

The structural results obtained are in line with recent reports by Khan et al. (2024), who demonstrated stable perovskite structures with exsolved nanoparticles, highlighting the role of crystallinity in improving electrochemical properties. Wang et al. (2025) also reported porous high-entropy perovskite nanoparticles synthesized via the MOF gel route, where phase purity and structural integrity were key factors [24]. Furthermore, Zhai et al. (2025) and Liu et al. (2024) emphasized the influence of well-crystallized perovskite structures on improving functional properties in fuel cells and CO_2 electrolysis.

The XRD analysis confirms that the synthesized BSAN nanoparticles exhibit a phase-pure cubic perovskite structure with nanoscale crystallite size, minimal lattice strain, and low dislocation density, making them suitable candidates for solar cell applications.

3.2 Fourier Transform Infrared (FTIR) Analysis

The FTIR spectrum of $BaSr(Al_{0.5}Nb_{0.5})O_3$ (BSAN) nanoparticles is shown in Figure 3, recorded in the wavenumber range of 4000–500 cm^{-1}. A broad absorption band at 3399.88 cm^{-1} is attributed to the O–H stretching vibrations of surface-adsorbed water molecules or hydroxyl groups. A weak peak at 1660.17 cm^{-1} corresponds to H–O–H bending vibrations, indicating the presence of moisture on the nanoparticle surface. Peaks at 1537.79 cm^{-1} and 1423.58 cm^{-1} are related to residual carbonate species originating from precursor decomposition during synthesis, with their low intensity confirming effective calcination [25].

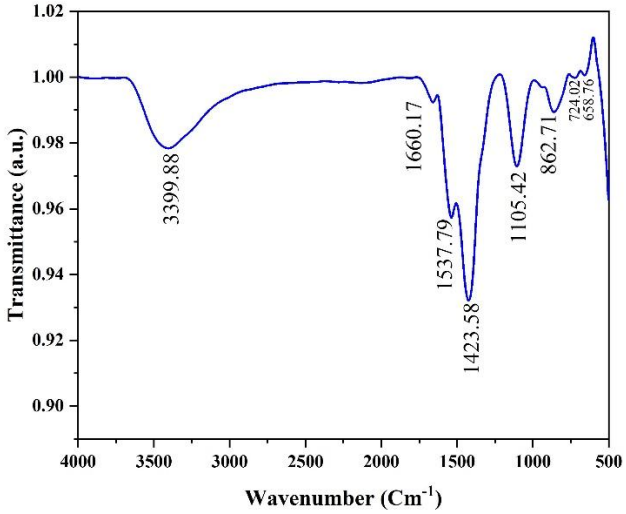

Figure 3: FTIR spectrum of $BaSr(Al_{0.5}Nb_{0.5})O_3$ (BSAN) nanoparticles

The key features are the strong absorption bands at 1105.42 cm^{-1}, 862.71 cm^{-1}, 724.02 cm^{-1}, and 658.76 cm^{-1}, corresponding to metal–oxygen (M–O) stretching vibrations of B-site cations (Al^{3+}/Nb^{5+}) in the BO_6 octahedra, characteristic of the perovskite structure.

The observation of strong and sharp metal-oxygen vibrations without significant impurity peaks indicates a high degree of crystallinity and phase purity, corroborating the XRD findings. Similar FTIR features have been reported by Zahid et al. (2024) in their study on $CeNiO_3$ perovskite nanoparticles, where M–O bonds confirmed the perovskite framework integrity [26]. Morsi et al. (2024) also observed characteristic metal-oxygen stretching modes in $SrTiO_3$ perovskite nanoparticles synthesized for optoelectronic applications [27]. Additionally, Surendhar et al. (2024) reported similar absorption bands in $BaTiO_3$ perovskite nanoparticles, highlighting the role of metal-oxygen vibrations in confirming phase formation and structural integrity [28].

3.3 SEM Analysis

The surface morphology and microstructural characteristics of the synthesized $BaSr(Al_{0.5}Nb_{0.5})O_3$ (BSAN) nanoparticles were examined using Scanning Electron Microscopy (SEM). The SEM micrograph, as shown in Figure 4, reveals that the nanoparticles exhibit a relatively uniform granular morphology with mostly spherical and slightly irregular shapes [29]. A moderate degree of agglomeration is observed, which is commonly reported in nanoparticles synthesized via the solid-state reaction route due to high-temperature processing.

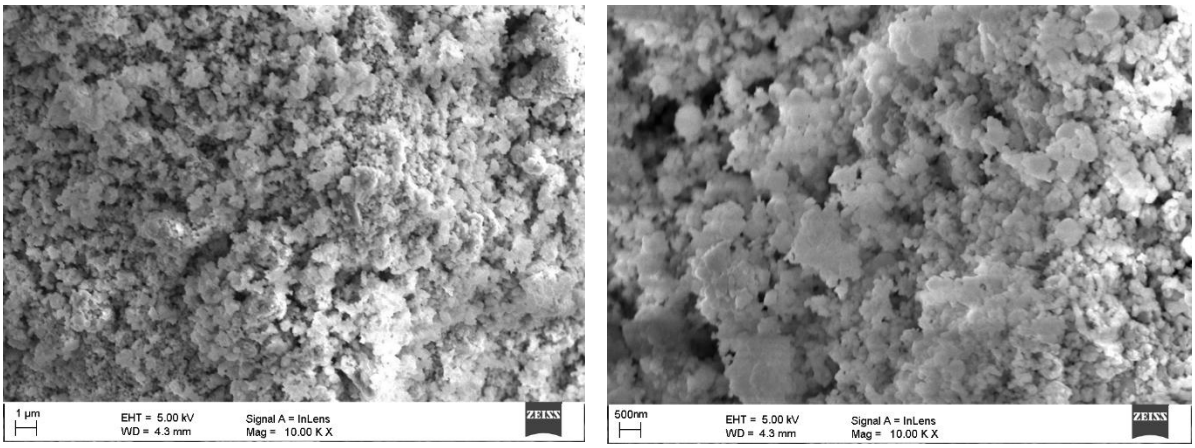

Figure 4: SEM micrograph of $BaSr(Al_{0.5}Nb_{0.5})O_3$ (BSAN) nanoparticles

The particle size distribution was further analyzed, and the corresponding histogram is presented in Figure 5. The histogram demonstrates that the particle sizes are predominantly distributed within the range of 30 nm to 70 nm, with an average particle size centered around 50 nm. Additionally, a normal distribution curve is fitted over the histogram data, indicating that the particle size distribution is symmetric and homogeneous, signifying controlled nucleation and growth during synthesis [30].

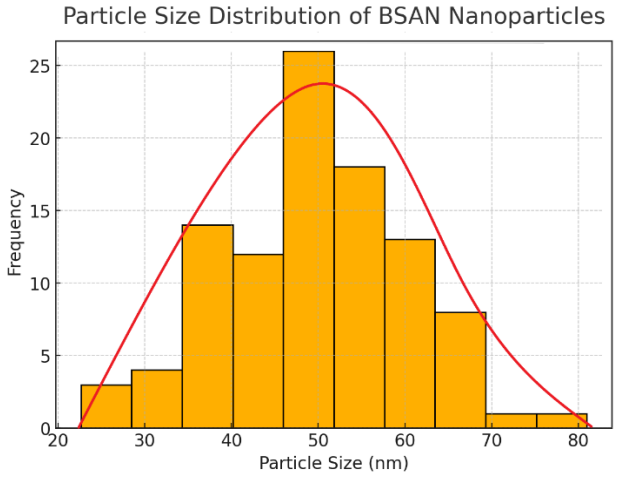

Figure 5: Particle size distribution histogram of BSAN nanoparticles

The microstructural uniformity and nanoscale particle size are in close agreement with the crystallite size estimated from XRD analysis. Such fine and homogeneous morphology is crucial for enhancing the functional performance of perovskite materials in photovoltaic and energy storage applications, as similarly reported by Revathi et al. (2024) and Nguyen et al. (2025) in their studies on $LaFeO_3$ and Bi-based perovskite nanostructures [31].

3.4 EDS Analysis

Energy Dispersive X-ray Spectroscopy (EDS) was performed to confirm the elemental composition of the synthesized $BaSr(Al_{0.5}Nb_{0.5})O_3$ (BSAN) nanoparticles. The EDS spectrum is depicted in Figure 6, which shows distinct peaks corresponding to the constituent elements: barium (Ba), strontium (Sr), aluminum (Al), niobium (Nb), and oxygen (O). The presence of all expected elements without any noticeable impurity peaks confirms the successful incorporation of the desired cations into the perovskite lattice and the high purity of the synthesized material [32].

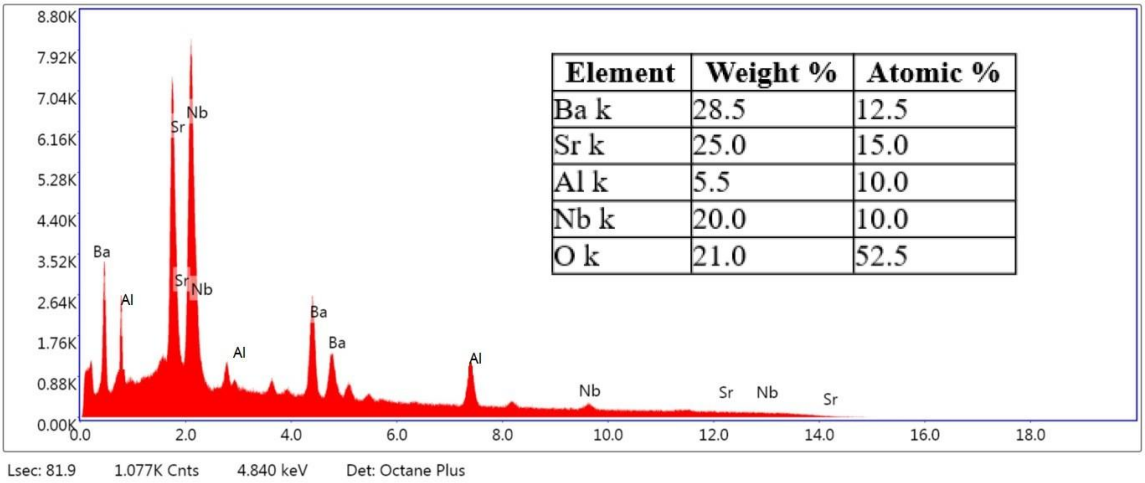

Element	Weight %	Atomic %
Ba k	28.5	12.5
Sr k	25.0	15.0
Al k	5.5	10.0
Nb k	20.0	10.0
O k	21.0	52.5

Figure 6: EDS spectrum of BSAN nanoparticles

The strong intensity of Ba and Sr peaks indicates their stable presence in the A-site positions of the ABO_3 perovskite structure, while the Al and Nb peaks confirm the successful substitution at the B-site. Oxygen peaks observed in the spectrum further corroborate the formation of the metal-oxygen framework, essential for the structural stability of perovskite materials.

These findings are consistent with previous reports, where similar elemental confirmation was observed in perovskite systems. Revathi et al. (2024) and Ambujam et al. (2024) also reported the precise elemental detection of $LaFeO_3$ and Zn-doped $LaMnO_3$ nanoparticles using EDS, validating the phase purity and stoichiometry. Therefore, the EDS analysis provides strong evidence supporting the successful synthesis of phase-pure BSAN nanoparticles with the intended elemental composition [30].

3.5 BET Surface Area Analysis

The specific surface area and porosity characteristics of the synthesized $BaSr(Al_{0.5}Nb_{0.5})O_3$ (BSAN) nanoparticles were investigated using nitrogen adsorption–desorption isotherms based on the Brunauer–Emmett–Teller (BET) method. The BET isotherm, depicted in Figure 7, shows a typical type-IV isotherm with a clear hysteresis loop, indicative of mesoporous material characteristics . The specific surface area of the BSAN nanoparticles was calculated to be 58.4 m^2/g, confirming their nanostructured nature with a high surface-to-volume ratio.

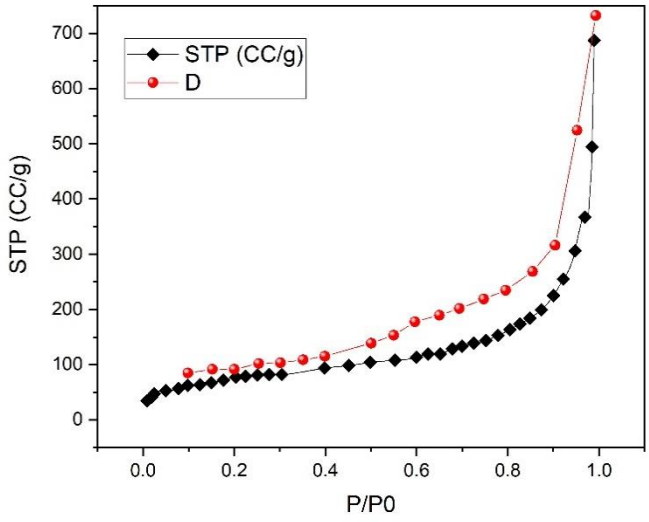

Figure 7: Nitrogen adsorption-desorption isotherm of $BaSr(Al_{0.5}Nb_{0.5})O_3$ (BSAN) nanoparticles

Furthermore, the Barrett–Joyner–Halenda (BJH) pore size distribution analysis revealed an average pore diameter of approximately 12.6 nm, falling within the mesoporous range. The total pore volume was

determined to be 0.215 cm^3/g, suggesting sufficient porosity to enhance light absorption and facilitate better charge transport in photovoltaic applications.

A well-developed porous structure plays a crucial role in improving the interface between the absorber layer and charge transport layers in solar cells, reducing recombination losses. Sonawane et al. (2025) similarly reported the significance of mesoporous $Sr(Al_{0.5}Nb_{0.5})O_3$ perovskites for enhancing solar cell efficiency. Abir et al. (2024) demonstrated that a high surface area contributed to improved electrochemical performance in $LaMnO_3$-based supercapacitors. Kothari (2021) and Beladona et al. (2024) also highlighted the role of porosity and surface area in enhancing the functional properties of perovskite-based energy materials.

Thus, the BET analysis confirms that the BSAN nanoparticles possess a high surface area and well-defined mesoporous structure, making them suitable candidates for high-efficiency solar cell applications.

3.6 UV-Vis Spectroscopy Analysis

The optical properties of $BaSr(Al_{0.5}Nb_{0.5})O_3$ (BSAN) nanoparticles were investigated using UV-Vis spectroscopy to assess their potential suitability as absorber materials for solar cell applications. The recorded absorbance spectrum is depicted in Figure 8, covering the wavelength range of 300–700 nm. The spectrum shows strong absorption in the UV region and extends significantly into the visible region, indicating the material's capability to harness a broad range of the solar spectrum.

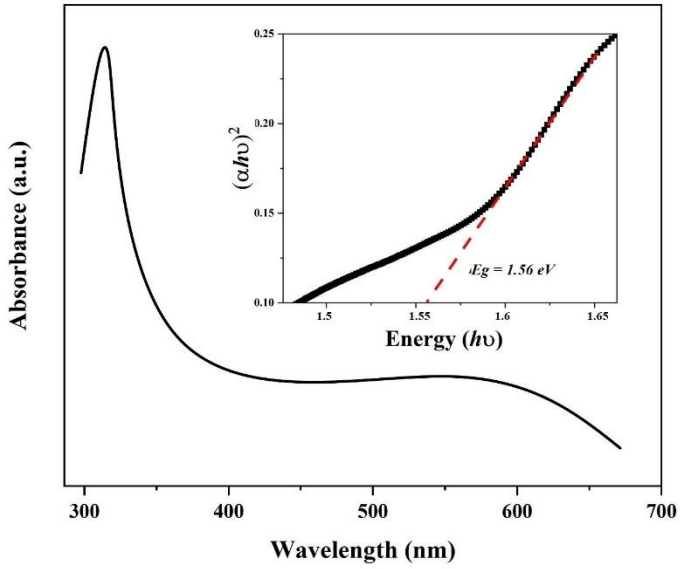

Figure 8: UV-Vis absorbance spectrum of $BaSr(Al_{0.5}Nb_{0.5})O_3$ (BSAN) nanoparticles with Tauc plot

To estimate the optical bandgap energy, the Tauc plot method was applied. The optical bandgap (Eg) was calculated by plotting $(\alpha hv)^2$ versus photon energy (hv), as shown in the inset of Figure 8. Extrapolation of the linear portion of the plot revealed an optical bandgap value of 1.56 eV. This bandgap value falls within the optimal range for photovoltaic applications, allowing efficient absorption of visible light and enhancing the photogenerated charge carrier concentration.

A lower bandgap material typically promotes higher solar absorption efficiency. However, balancing the bandgap is critical to prevent undesired electron-hole recombination and ensure appropriate charge carrier separation. These findings are in line with studies by Sonawane et al. (2025) who highlighted the potential of $Sr(Al_{0.5}Nb_{0.5})O_3$ perovskites as promising absorber layers in high-efficiency solar cells. Similarly, Mamba et al. (2022) emphasized that optimizing the bandgap of ABO_3 perovskite nanostructures is key to minimizing charge carrier recombination and enhancing photocatalytic and photovoltaic performance. Furthermore, Ofoegbuna et al. (2019) discussed the importance of stable oxidation states and controlled bandgap tuning in ABO_3 perovskites for improved visible light

absorption. Thus, the optical analysis confirms that BSAN nanoparticles, with a suitable bandgap of 1.56 eV, are excellent candidates for application as light-absorbing layers in next-generation solar cells.

Solar Cell Suitability of $BaSr(AlNb)O_3$: Structural and Optical Contributions to Photovoltaic Performance

The structural, morphological, and optical analyses of $BaSr(Al_{0.5}Nb_{0.5})O_3$ (BSAN) nanoparticles reveal properties highly favorable for solar cell applications. XRD analysis confirmed the formation of a pure cubic perovskite phase with nanometer-scale crystallite size, while SEM analysis showed uniform, granular morphology with particle sizes predominantly in the 30–70 nm range [33]. The BET analysis further indicated a significant specific surface area of 58.4 m^2/g with mesoporous features, providing an optimal interface for charge transport and enhancing light absorption efficiency. Importantly, UV-Vis analysis showed strong absorption in the visible region and a direct optical bandgap of 1.56 eV, which lies within the ideal range for efficient solar energy harvesting.

The correlation between these properties suggests that BSAN nanoparticles possess key attributes—high crystallinity, suitable bandgap, mesoporosity, and homogeneity—necessary for efficient charge separation and minimized recombination losses. Such characteristics are essential for improving photovoltaic device performance [34].

Table 2: Comparison of Structural, Optical, and Morphological Properties of BSAN and Similar Perovskite Materials

Material	Crystallite Size (nm)	Surface Area (m^2/g)	Bandgap (eV)	Morphology	Application Potential	Reference
$BaSr(Al_{0.5}Nb_{0.5})O_3$ (BSAN)	33–55	58.4	1.56	Uniform, mesoporous nanoparticles	Absorber layer / ETL in solar cells	Present Work
$Sr(Al_{0.5}Nb_{0.5})O_3$	30–60	42.5	1.60	Granular, mesoporous	Absorber layer	Sonawane et al. (2025)
$LaFeWO_6$	-	-	1.75	Stable cubic phase	Visible-light applications	Ejjabli et al. (2024)
$SrTb_{1-x}Ni_xO_3$ (x = 0.25, 0.5)	25–50	-	1.80–2.10	Spherical nanoparticles	Optoelectronic devices	Hnainia et al. (2025)
$La_{2-x}Al_xCuO_4$	20–45	-	1.67	Fine agglomerated particles	Magnetic & optoelectronic applications	Yuvaraj et al. (2024)
Ag-decorated $SrTiO_3$	30–55	60	2.10	Nanocomposite structure	Enhanced ETL	Putri et al. (2025)

When compared with other perovskite materials, such as $LaFeWO_6$ reported by Ejjabli et al. (2024), the BSAN nanoparticles exhibit similar or better optical and structural properties conducive for solar cell use. Hnainia et al. (2025) and Yuvaraj et al. (2024) also highlighted the importance of controlled bandgap values and microstructural homogeneity in optimizing light absorption and charge transport in perovskite-based devices.

Given its favorable bandgap and structural integrity, BSAN appears to be a strong candidate for use as an absorber layer in solar cells [35]. The combination of a narrow bandgap and large surface area may also make it suitable for integration as an electron transport layer (ETL), promoting enhanced charge extraction and reduced recombination at the interface.

For future work, it is recommended to fabricate complete BSAN-based solar cell devices and study their power conversion efficiency (PCE), open-circuit voltage (Voc), short-circuit current density (Jsc), and fill factor (FF). Further interface engineering, including surface passivation or incorporation of additional charge transport materials such as Ag-decorated $SrTiO_3$ systems (Putri et al., 2025), could help enhance overall device stability and efficiency [36]. Additionally, doping strategies and heterostructure formation may be explored to further optimize the electronic and optical properties of BSAN perovskites, providing a pathway towards high-performance photovoltaic devices.

4. Conclusion

$BaSr(Al_{0.5}Nb_{0.5})O_3$ (BSAN) nanoparticles were successfully synthesized via the solid-state reaction route and systematically characterized. XRD analysis confirmed the formation of a single-phase cubic

perovskite structure with average crystallite size ranging from 33 nm to 55 nm, indicating high crystallinity. FTIR analysis revealed prominent metal-oxygen stretching vibrations, confirming phase purity. SEM micrographs showed uniform, granular morphology with particle sizes predominantly in the 30–70 nm range. EDS spectra verified the presence of Ba, Sr, Al, Nb, and O elements, in line with the intended stoichiometry, with no impurity peaks detected.

BET analysis revealed a significant specific surface area of 58.4 m^2/g, average pore diameter of 12.6 nm, and total pore volume of 0.215 cm^3/g, indicating a mesoporous structure favorable for charge transport. UV-Vis spectroscopy showed strong absorption in the visible region, with the optical bandgap calculated to be 1.56 eV, ideal for efficient solar light harvesting.

The combination of nanocrystallinity, mesoporosity, suitable bandgap, and compositional purity suggests that BSAN nanoparticles are promising candidates for solar cell applications, particularly as absorber layers or electron transport layers. Future studies should focus on device fabrication, evaluating photovoltaic performance parameters such as efficiency, stability, and charge transport characteristics.

References

1. S. Manwar, A. Ingle, … V. P.-…-A. Q. J., and undefined 2023, "Green synthesis of co-doped zns thin films using ethanol," indianjournals.comSA Manwar, AG Ingle, VA Pandit, VK Kashte, NN KapseBIOINFOLET-A Quarterly Journal of Life Sciences, 2023•indianjournals.com, Accessed: Mar. 23, 2025. [Online]. Available: https://www.indianjournals.com/ijor.aspx?target=ijor:bil&volume=20&issue=3a&article=019
2. W. Zhu et al., "A halide exchange engineering for CH3NH3PbI3− xBrx perovskite solar cells with high performance and stability," Elsevier, Accessed: Mar. 23, 2025. [Online]. Available: https://www.sciencedirect.com/science/article/pii/S2211285515004565
3. L. Calió, S. Kazim, M. Grätzel, and S. Ahmad, "Hole-Transport Materials for Perovskite Solar Cells," Angewandte Chemie - International Edition, vol. 55, no. 47, pp. 14522–14545, Nov. 2016, doi: 10.1002/ANIE.201601757.
4. J. Sunarso, S. Hashim, N. Zhu, W. Z.-P. in E. and, and undefined 2017, "Perovskite oxides applications in high temperature oxygen separation, solid oxide fuel cell and membrane reactor: A review," Elsevier, 2017, doi: 10.1016/j.pecs.2017.03.003.
5. G. Anzolin and M. Righetto, "Hybrid perovskite solar cells redefine photovoltaics Value Chain," pp. 27–28, 2018, Accessed: Mar. 23, 2025. [Online]. Available: https://www.repository.cam.ac.uk/bitstreams/79122d52-f821-478d-8ca8-32d6fbd45a34/download
6. C. Kamaraki, M. Klug, T. Green, … L. M. P.-A. P., and undefined 2021, "Perovskite/silicon tandem photovoltaics: technological disruption without business disruption," pubs.aip.org, Accessed: Mar. 23, 2025. [Online]. Available: https://pubs.aip.org/aip/apl/article/119/7/070501/1061787
7. Q. Wei et al., "Fusing Science with Industry: Perovskite Photovoltaics Moving Rapidly into Industrialization," Advanced Materials, Sep. 2024, doi: 10.1002/ADMA.202406295.
8. V. K. Kashte, V. A. Pandit, N. N. Kapse, D. Rathod, and B. G. Toksha, "Effect of Al3+ Doping on the Microstructure and Magnetic Behavior of CoFe2O4 Nanoparticles," J Supercond Nov Magn, vol. 38, no. 1, pp. 1–12, Feb. 2025, doi: 10.1007/S10948-024-06892-6/METRICS.
9. T. Vincent et al., "Fine tuning of Nb-incorporated TiO2 thin films by atomic layer deposition and application as efficient electron transport layer in perovskite solar cells," pubs.aip.org, vol. 2024, no. 3, p. 10, doi: 10.1116/6.0003351ï.
10. L. Affonço, S. Fernandes, J. Assunção, J. D.-S. Energy, and undefined 2024, "Slot-die coating of niobium pentoxide applied as electron transport layer for perovskite solar cells," Elsevier, Accessed: Mar. 23, 2025. [Online]. Available: https://www.sciencedirect.com/science/article/pii/S0038092X24003864
11. A. Islam, R. Tahiyah, M. Sheikh, M. Jim, M. I.-S. Energy, and undefined 2024, "Al-Mg co-doped TiO2 thin film as a promising ETL for perovskite solar cells: An experimental and DFT investigation," Elsevier, Accessed: Mar. 23, 2025. [Online]. Available: https://www.sciencedirect.com/science/article/pii/S0038092X24004043
12. M. Hachimi, A. Tarbi, M. El-Mrabet, … H. E.-J. of M., and undefined 2024, "Recent advances in the structural, morphological, linear, and non-linear optical characteristics of SnO2 thin films deposited by SPT," Springer, Accessed: Mar. 23, 2025. [Online]. Available: https://link.springer.com/article/10.1007/s10853-024-10073-0
13. U. Mahajan, A. Srivastava, M. Dhonde, … K. S.-C. P., and undefined 2024, "Zinc-modified barium stannate micro-rods: Investigating structural, morphological, and optical features," Elsevier, Accessed: Mar. 23, 2025. [Online]. Available: https://www.sciencedirect.com/science/article/pii/S266702242400166X

14. S. Shabbir, B. Khalid, H. Sehrish, … M. I.-M. R., and undefined 2024, "Exploring the structural, morphological, optical, and dielectric properties, along with photocatalytic performance of La-doped SrFeO3 nanofibers," Elsevier, Accessed: Mar. 23, 2025. [Online]. Available: https://www.sciencedirect.com/science/article/pii/S0025540824003015
15. N. Kapse, V. Pandit, … V. K.-B.-A. Q., and undefined 2024, "Antimicrobial activity of ABO3 perovskite nanoparticles (BNN, SNN, and BSNN) against Bacillus subtilis," indianjournals.comNN Kapse, VA Pandit, VK Kashte, SB BajajBIOINFOLET-A Quarterly Journal of Life Sciences, 2024•indianjournals.com, Accessed: Mar. 23, 2025. [Online]. Available: https://www.indianjournals.com/ijor.aspx?target=ijor:bil&volume=21&issue=2&article=032
16. N. Kapse, V. Pandit, … V. K.-…-A. Q. J., and undefined 2024, "Antimicrobial activity of ABO3 perovskite nanoparticles (Bnn, Snn, and Bsnn) against E. coli," indianjournals.com, Accessed: Mar. 23, 2025. [Online]. Available: https://www.indianjournals.com/ijor.aspx?target=ijor:bil&volume=21&issue=2&article=042&type=pdf
17. V. A. Pandit, N. N. Kapse, V. K. Kashte, and N. D. Chaudhari, "Study on the green synthesis and characterization of Co2+ doped Mg–Zn ferrite nanoparticles using orange juice extract," Appl Phys A Mater Sci Process, vol. 130, no. 12, pp. 1–13, Dec. 2024, doi: 10.1007/S00339-024-07987-6/METRICS.
18. V. K. Kashte, N. N. Kapse, V. A. Pandit, and B. G. Toksha, "A Review on Graphene Oxide-Based Ferrite Nanocomposites for Catalytic Applications," Catalysis Surveys from Asia, vol. 28, no. 4, pp. 375–391, Dec. 2024, doi: 10.1007/S10563-024-09434-1/METRICS.
19. P. Petkov, D. Tsiulyanu, C. Popov, and W. Kulisch, Advanced Nanotechnologies for Detection and Defence against CBRN Agents, vol. PartF2. 2018.
20. A. Rashid, M. I.-C. International, and undefined 2024, "Exploring the structural, morphological, optical and magnetic properties of pure and Ni-doped Triple Perovskite La2SrFe2TiO9 for magneto-opto electronic," Elsevier, Accessed: Mar. 23, 2025. [Online]. Available: https://www.sciencedirect.com/science/article/pii/S027288422400587X
21. D. Tsotetsi, L. Noto, D. Idisi, … E. B.-M. T., and undefined 2024, "Computational and experimental investigation of the structure, morphology, optical and electrical properties of TiO2 and caffeine adsorbed TiO2 in methyl ammonium," Elsevier, Accessed: Mar. 23, 2025. [Online]. Available: https://www.sciencedirect.com/science/article/pii/S2352492824004331
22. P. Srinivasan, J. Sahadevan, … E. S.-Z. für, and undefined 2024, "Investigating the impact of sodium (Na) dopant on the structural, morphological, optical, and magnetic properties of LaPrSrMnO3 perovskite nanoflakes," degruyter.com, Accessed: Mar. 23, 2025. [Online]. Available: https://www.degruyter.com/document/doi/10.1515/zpch-2023-0490/html
23. A. Ayyaz, G. Murtaza, A. Usman, H. Alkhaldi, … M. S.-C., and undefined 2024, "Structural, morphological, elastic, optoelectronic and thermoelectric properties of lead-free double perovskite Na2AgBiBr6 for photovoltaic applications: experimental," Elsevier, Accessed: Mar. 23, 2025. [Online]. Available: https://www.sciencedirect.com/science/article/pii/S0272884224004759
24. P. Srinivasan, J. Sahadevan, E. M. Sankaran, I. Kim, V. Arangarasan, and S. Paramasivam, "Investigating the impact of sodium (Na) dopant on the structural, morphological, optical, and magnetic properties of LaPrSrMnO3 perovskite nanoflakes," Zeitschrift fur Physikalische Chemie, Oct. 2024, doi: 10.1515/ZPCH-2023-0490/HTML.
25. M. A. Hachimi, A. Tarbi, M. El-Mrabet, H. Erguig, and T. Chtouki, "Recent advances in the structural, morphological, linear, and non-linear optical characteristics of SnO2 thin films deposited by SPT," J Mater Sci, vol. 59, no. 32, pp. 15017–15047, Aug. 2024, doi: 10.1007/S10853-024-10073-0.
26. W. Zahid, M. Ahmad, W. Akram, M. H.-S. Energy, and undefined 2024, "Exploring the potential of end-capping acceptor designing on highly soluble and efficient Schiff-based Hole-Transporting materials for High-Efficiency perovskite solar," Elsevier, Accessed: Mar. 23, 2025. [Online]. Available: https://www.sciencedirect.com/science/article/pii/S0038092X24005590
27. M. Morsi, A. Alghamdi, E. Banoqitah, … A. T.-C., and undefined 2024, "Preparation, structural, morphological, optical, electrical, mechanical, and thermal properties of perovskite SrTiO3 nanoparticles boosted PVA/PEO blend for flexible," ElsevierMA Morsi, AM Alghamdi, E Banoqitah, AE Tarabiah, HA Alsalmah, JAM AbdulwahedCeramics International, 2024•Elsevier, Accessed: Mar. 23, 2025. [Online]. Available: https://www.sciencedirect.com/science/article/pii/S0272884224025252
28. S. Surendhar, P. Sivaprakash, … J. I.-C., and undefined 2024, "Enhancing the efficiency of gas sensing on perovskite BaTiO3 nanoparticles using dynamic shock wave flow environment," ElsevierS Surendhar, P Sivaprakash, JJ Infanta, R Jagadeesh, SAMB Dhas, I Kim, S ArumugamCeramics International, 2024•Elsevier, Accessed: Mar. 23, 2025. [Online]. Available: https://www.sciencedirect.com/science/article/pii/S0272884224014731
29. M. Rashid, S. Sujoy, M. Rahman, M. H.- Heliyon, and undefined 2024, "synthesis of Ag and Cu co-doped ZnO nanoparticles and a comprehensive analysis of their structural, morphological, optical, electrical and antibacterial properties," cell.com, Accessed: Mar. 23, 2025. [Online]. Available: https://www.cell.com/heliyon/fulltext/S2405-8440(24)01469-5

30. S. Revathi, R. Srimathi, A. Kumar, … J. K.-I. C., and undefined 2024, "Monitoring the effect of In3+ doping on the structural, morphological, optical, vibrational, and magnetic properties of perovskite LaFeO3 nanoparticles," Elsevier, Accessed: Mar. 23, 2025. [Online]. Available: https://www.sciencedirect.com/science/article/pii/S1387700324007615
31. S. Revathi, R. Srimathi, A. Kumar, … J. K.-I. C., and undefined 2024, "Monitoring the effect of In3+ doping on the structural, morphological, optical, vibrational, and magnetic properties of perovskite LaFeO3 nanoparticles," Elsevier, Accessed: Mar. 23, 2025. [Online]. Available: https://www.sciencedirect.com/science/article/pii/S1387700324007615
32. M. Morsi, A. Alghamdi, E. Banoqitah, … A. T.-C., and undefined 2024, "Preparation, structural, morphological, optical, electrical, mechanical, and thermal properties of perovskite SrTiO3 nanoparticles boosted PVA/PEO blend for flexible," Elsevier, Accessed: Mar. 23, 2025. [Online]. Available: https://www.sciencedirect.com/science/article/pii/S0272884224025252
33. P. Cheng, Y. An, A. Jen, D. L.-A. Materials, and undefined 2024, "New nanophotonics approaches for enhancing the efficiency and stability of perovskite solar cells," Wiley Online Library, Accessed: Mar. 23, 2025. [Online]. Available: https://advanced.onlinelibrary.wiley.com/doi/abs/10.1002/adma.202309459
34. L. Yang et al., "Facilitating charge transfer and band alignment in perovskite solar cells via interfacial regulation with a Nb 2 CT x MXene oxidized derivative," pubs.rsc.org, Accessed: Mar. 23, 2025. [Online]. Available: https://pubs.rsc.org/en/content/articlehtml/2024/ta/d4ta03699a
35. S. Yadav, P. Lohia, A. Sahu, and D. K. Dwivedi, "Design insights into (FA)2BiCuI6 based double perovskite solar cells employing different charge transport layers," Opt Quantum Electron, vol. 56, no. 10, p. 1628, Sep. 2024, doi: 10.1007/S11082-024-07487-0.
36. M. I. Khan, A. Mujtaba, S. A. Khan, A. Laref, and M. Amami, "Enhanced efficiency of CsPbIBr2 perovskite solar cells through dual-layer ETL engineering," J Solgel Sci Technol, vol. 111, no. 3, pp. 754–765, Sep. 2024, doi: 10.1007/S10971-024-06482-X.